JOURNAL OF CATALYSIS 20, 88–96 (1971)

Synthetic Offretite

I. Physicochemical Characterization

T. E. WHYTE, JR., E. L. WU, G. T. KERR, AND P. B. VENUTO

Mobil Research and Development Corporation, Research Department, Paulsboro, New Jersey 08066

Received April 13, 1970

The thermochemical, crystallographic, morphologic and catalytic properties of a synthetic tetramethylammonium (TMA) offretite and its ammonium and hydrogen derivative forms have been investigated. TMA offretite crystallizes as small irregular particles ($0.5\,\mu \times 1.5\,\mu$) in contrast to the more elongated crystals of natural and synthetic erionite. Thermal decomposition of TMA ions (probably located in the large intracrystalline pores along the *c* crystallographic axis) occurs near 483°C. The resulting catalyst sorbs 7.8 wt % cyclohexane, 8.8 wt % *n*-hexane and 16.5 wt % water. Room temperature ion exchange of the parent TMA offretite with 0.1 *N* $(NH_4)_2SO_4$ yields an ammonium derivative with one potassium per unit cell trapped in a cancrinite cage or hexagonal prism. Conversion of NH_4-offretite to the acid form requires a temperature 100°C higher than NH_4Y. Acid offretite shows significant activity for the catalytic cracking of *n*-hexane.

INTRODUCTION

Gonnard (*1*) in 1890 described a new zeolite, offretite, occurring very sparingly with phillipsite in the basalt of Mt. Semiouse, Montbreson, Loire, France. Erionite existing in rhyolite–tuff was discovered in 1896 by Eakle (*2*) in Durkee, Oregon. Considerable confusion followed in the literature (*3*), (*4*) concerning the relationship between offretite and erionite. However, Bennett and Gard (*5*), using electron diffraction and single crystal X-ray analysis, demonstrated that offretite and erionite had closely related but distinctly different structures. They further observed that the two could intergrow, citing Linde T as an example.

Although the physical, chemical and catalytic properties of erionite have been explored extensively (*6–16*), little or no information has been reported on the closely related zeolite, offretite. We now report the results of an investigation into the physicochemical properties—including thermochemical, crystallographic, morphologic, and catalytic aspects of a synthetic tetramethylammonium (TMA) offretite and its ammonium and hydrogen derivative forms.

EXPERIMENTAL

Synthetic Offretite

Tetramethylammonium (TMA) offretite was synthesized from an alumina–silica gel in the presence of potassium, sodium and tetramethylammonium hydroxides by the method of Rubin (*17*). The ammonium form of offretite was generated by air calcination of TMA offretite for 16 hr, at 600°C, followed by four room temperature exchanges with 0.1 *N* $(NH_4)_2SO_4$. The unit cell compositions and analytical data of the resulting TMA and ammonium forms are given in Table 1.

Apparatus and Procedures

Thermal analyses were performed using Dupont 900 and 950 differential thermal

TABLE 1
ANALYTICAL DATA FOR TMA AND AMMONIUM OFFRETITE

Catalyst[a]	Composition	Surface area (m^2/g), BET	Sorption[b] (g/100 g catalyst)		
			Water	Cyclohexane	*n*-Hexane
		$(P/P_0)^{25°C}$ =	0.50	0.20	0.13
TMA Offretite	$[(CH_3)_4N]^c_{0.07}(Na)_{0.20}(K)_{0.73}(AlO_2)_{1.00}(SiO_2)_{4.13}$	339	16.5	7.8	8.8
NH_4 Offretite	$(NH_4)_{0.76}(K)_{0.23}(Na)_{0.02}(AlO_2)_{1.00}(SiO_2)_{3.85}$	467	21.4	7.2	10.8

[a] Loss on ignition, 10 min/1000°C/air, 15.9%(TMA-offretite) or 20.6% (NH_4-offretite); samples equilibrated over sat. $(NH_4)_2SO_4$ at room temperature $P^{25°C}_{H_2O}$ = 19.1 mm Hg prior to ignition.

[b] Ignited 16 hr/air at 483°C (TMA-offretite) or 350°C (NH_4-offretite) before sorption.

[c] Calculated on basis of alkali metal-free AlO_2 units; observed analysis (C, 4.46 wt %; N, 1.09 wt %) corresponds to $(CH_3)_4N/Al$ ratio of 0.31; this excess of $(CH_3)_4N$ is attributed to $(CH_3)_4NOH$ occluded within zeolite pores.

(DTA) and thermal gravimetric (TGA) analyzers. The TGA apparatus had been previously modified to allow acid titration (NH_2SO_3H) of any basic decomposition products from the TGA effluent stream. X-ray patterns were obtained using a Siemens Powder Diffractometer with strip chart recorder and pulse height analyzer. Electron microscopic examinations were carried out using an RCA EMU-3 microscope.

X-ray Analysis and Structure

Electron diffraction and X-ray single crystal studies (*5*) have shown that both erionite and offretite are hexagonal. The lattice parameters of offretite are a = 13.31 Å, c = 7.59 Å, that is with c one-half that of erionite. Hence, the most prominent difference in the X-ray diffraction patterns of erionite and offretite is the absence of diffraction peaks in the offretite pattern which have an odd l Miller index in the erionite pattern. These lines will be referred to as "odd l" lines. Line drawings of these two structures are shown in Figs. 1, 2, and 3. Offretite and erionite differ from one another by the manner in which the hexagonal rings and the hexagonal prisms (double six-membered rings) are arranged—the stacking sequence. Erionite, Fig. 1, consists of a layer of six-membered

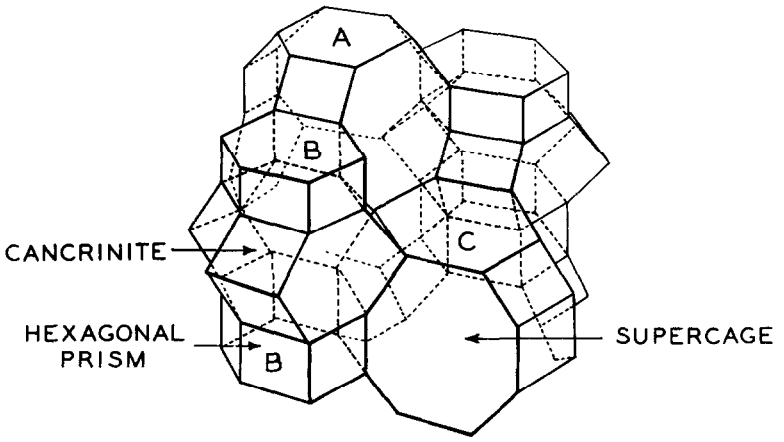

FIG. 1. Line drawing of cage and hexagonal layer system in erionite. Vertices represent Si or Al atoms; lines represent oxygens. Stacking sequence indicated by capital letters.

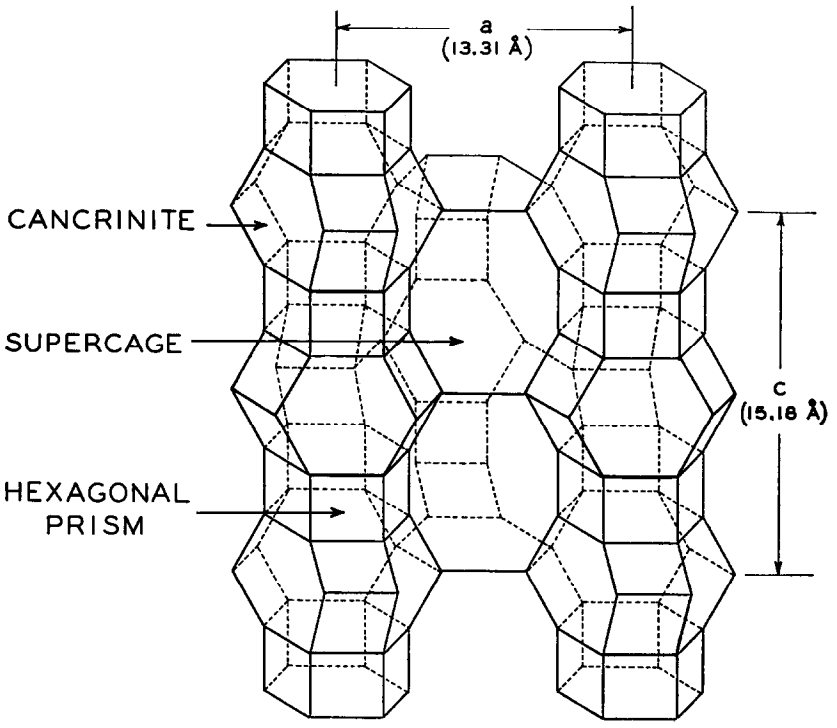

FIG. 2. Line drawing of erionite showing the crystallographic parameters.

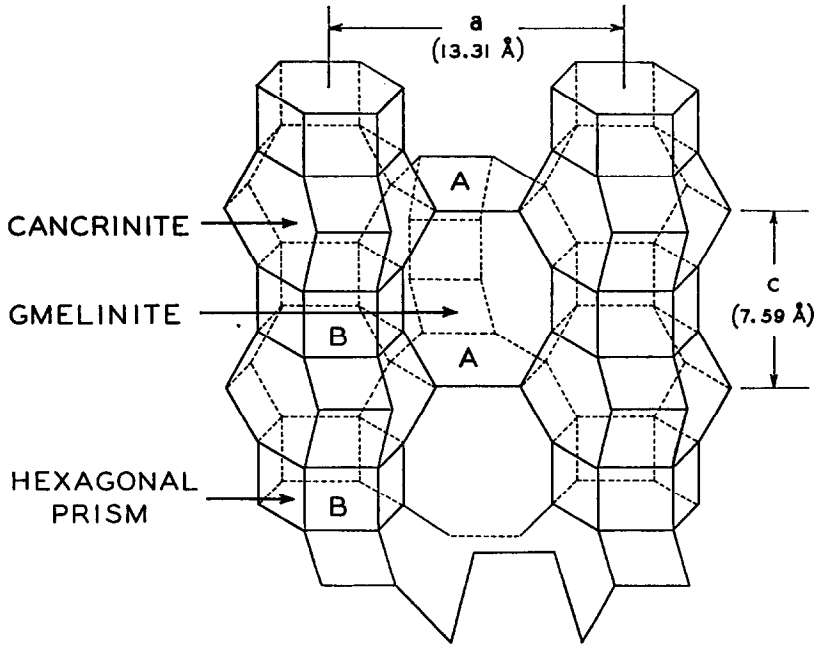

FIG. 3. Line drawing of cage and hexagonal layer system in offretite. Stacking sequence is indicated by capital letters.

rings, layer A; and a layer of hexagonal prisms, layer B. The next layer of single six-rings, layer C, is rotated through 60° relative to the first layer of six-membered rings. The stacking sequence is ABCBABCB. In offretite, Fig. 3, all layers of six-membered rings are superimposed, and therefore identical. These layers are stacked ABAB along the *c* directions in offretite.

Results and Discussion

X-ray Powder Diffractions Studies

The X-ray powder diffraction pattern of TMA offretite is presented in Fig. 4. Since offretite has a *c* parameter half that of erionite, all the odd *l* lines (indicated by * in Fig. 4) are missing. The presence, however, of a small number of disordered erionite layers would give rise to very weak "odd *l*" reflections which may not be observed in a normal powder pattern. Examination of reflections from the 101, 201, 211 and 311 "odd *l*" planes using X-ray step scanning techniques revealed the presence of very weak and narrow lines. This trace of erionite (<1%) did not interfere with the cyclohexane sorption capacity of the zeolite as 7.8 wt % is sorbed (Table 1), in contrast to only 1.0% in pure erionite (*9*).

Electron and Light Microscopy

The complete crystallization and growth of offretite takes three to four days. Although offretite and erionite have closely related structural configurations, their crystal habits are different. Photomicrographs of TMA offretite, natural erionite (*16*) and synthetic erionite (*18*) are presented in Fig. 5. Synthetic offretite (Fig. 5a) crystallizes as very small particles of irregular shape (0.5 μ in width and 1.5 μ in length) which seem to possess rounded edges. In contrast to this, natural erionite (Fig. 5b) grows in the shape of long, thin needles. Close examination of several larger rod-like particles indicates that they are agglomerates, composed of bundles of needle-like material. On the other hand, synthetic erionite (*18*), Fig. 5c, crystallizes in the form of short stubby rods, 10–15 μ long and 6 μ wide—often appearing with rounded edges.

Sorptive Properties of TMA-Offretite

The cationic composition (Na, K, TMA) in synthetic offretite is such that both the size and location of these ions in the intracrystalline pore system will affect the capacity for sorbing hydrocarbons. In offretite the two diffusional pathways are defined by channels along the *c* and *a* crys-

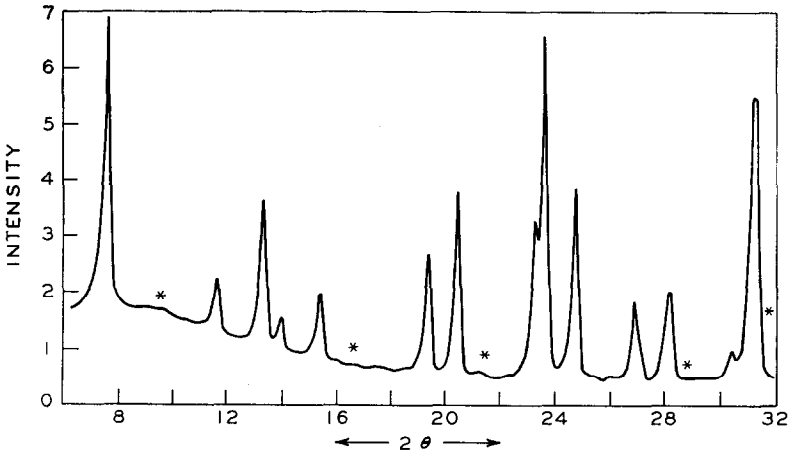

FIG. 4. X-ray powder diffraction pattern of TMA offretite. Regions where *l*, the Miller index is odd, are indicated by *.

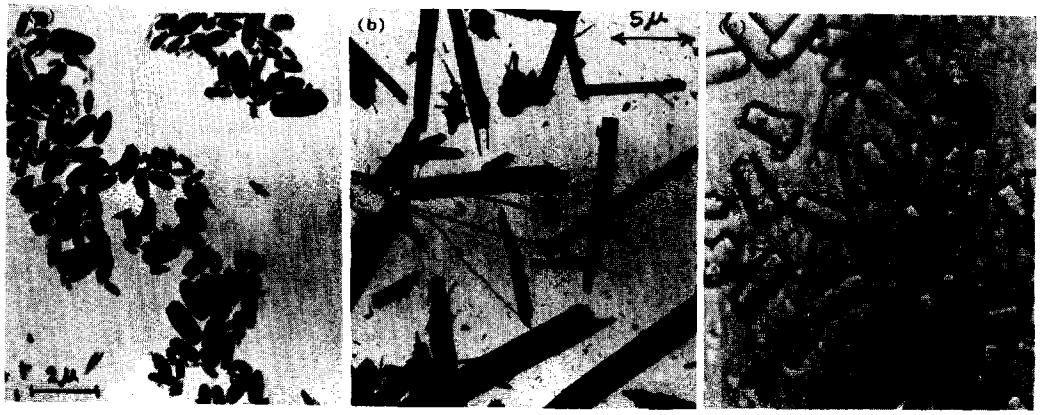

FIG. 5. Electon and light photomicrographs: (a) synthetic TMA offretite, (b) natural erionite, and (c) synthetic erionite.

tallographic axes with diameters of 6.3 Å and 4.5 Å, respectively. From the average cation occupancy per unit cell and their critical diameters, listed in Table 2, we can see that tetramethylammonium ions could effectively block the intra-crystalline pores for hydrocarbon sorption. To learn the extent to which tetramethylammonium ions could affect hydrocarbon sorptions, an *in situ* TGA calcination (decomposing TMA ions) and sorption experiments were performed. The results are presented in Table 3. We note that both the cyclohexane and *n*-hexane sorptions increased immensely, 16X and 6X, respectively, after calcination.

TABLE 2
DIMENSIONS OF CATIONS IN TMA OFFRETITE

Cation	Average number of cations per unit cell[a]	Diameter (Å)
$(CH_3)_4N^+$	0.3	6.94[b]
Na^+	0.7	1.90[c]
K^+	2.6	2.66[c]

[a] Calculated on the basis of 18 $(Si,Al)O_4$ per unit cell.

[b] Twice the sum of C–N bond distance (1.47 Å) and Van der Waal radius of CH_3 group (2.0 Å).

[c] Ionic radii for coordination number of 6.

TABLE 3
SORPTIVE PROPERTIES OF TMA OFFRETITE

Sorbate	Critical[c] diameter (Å)	Sorption (g/100 gm catalyst) $(P/P_0)^{25°C} \sim 1$: Before TMA decomposition[a]	Sorption (g/100 gm catalyst) $(P/P_0)^{25°C} \sim 1$: After TMA decomposition[b]
Water	2.8	11.6	14.1
Cyclohexane	6.0	0.6	9.2
n-Hexane	4.3	1.5	8.9

[a] Catalyst dried 16 hr/250°C/air in TGA before sorption.

[b] Catalyst heated 600°C/He in TGA until all TMA decomposed as indicated by acid titration.

[c] Diameters measured from Leybold atomic models.

The volume gained, 11cc of cyclohexane/100 g of catalyst (Table 3) (using $d^{20°}_{cyclohexane} = 0.779$), agrees well with the calculated volume of 9 cc/100 g of catalyst occupied originally by the TMA cations. Using the critical dimensions (column 2 of Table 3), we can gauge the effective pore diameter of this zeolite before calcination as >2.8 Å but <4.3 Å, and after calcination, as >6.0 Å.

The tetramethylammonium ions retained by the zeolite during crystallization seem to be located in the large intracrystalline pores along the *c* crystallographic axis where they effectively block or slow down significantly the sorption of hydrocarbons. An alternate explanation, blockage by potassium and/or sodium ions located in the large channels and TMA ions fixed in the small gmelinite cages is less likely.

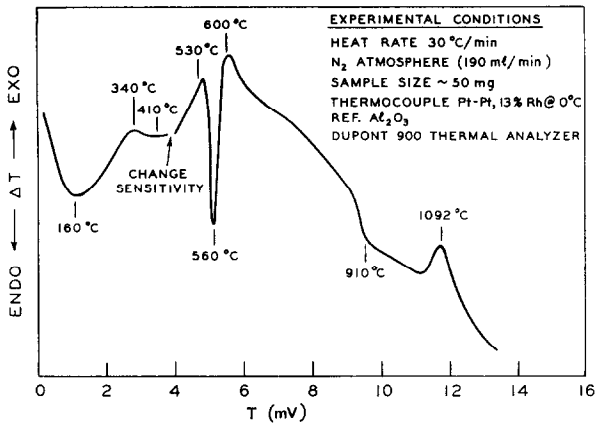

FIG. 6. DTA profile of tetramethylammonium offretite.

Thermal Analysis of Synthetic Offretite

1. Differential thermal analysis (DTA). Figure 6 shows the DTA profile of synthetic offretite. Inspection of the curve reveals several major transitions. The first endotherm at 160°C corresponds to loss of adsorbed water. The two endotherms at 410°C and 560°C reflect transformations relating to the decomposition of the $(CH_3)_4N^{\oplus}$ species. The slight inflection near 910°C does not arise from significant loss of crystallinity or a phase change, as indicated by X-ray examination of a sample removed from the DTA apparatus after heating to 965°C. The weak exotherm at 1092°C is associated with breakdown of the offretite lattice. X-ray examination of the sample after undergoing the transition at 1092°C showed it to be completely amorphous.

2. Thermogravimetric analysis (TGA). In an effort to relate the transitions assigned above to specific physical or chemical changes, TMA offretite was examined by thermogravimetric analysis. The main weight losses and the temperature ranges over which they occur are shown in Table 4 for triplicate determinations, together with confirmatory DTA correlations and probable assignments. Basic material, which was released over the temperature range 350–575°C, was quantitatively titrated with sulfamic acid.

Let us assume that all the intracrystalline tetramethylammonium cations, $(CH_3)_4N^{\oplus}$, in this offretite decompose according to the following stoichiometry:

$$[(CH_3)_4N^{\oplus}\,{}^{\ominus}O\text{—}Al\text{—}OSi] \rightarrow (CH_3)_3N + [CH_2] + HO\text{—}Al\text{—}OSi. \quad (1)$$

The quantities of basic material evolved as determined by acid titration, were 2.7,

TABLE 4
THERMOGRAVIMETRIC ANALYSIS OF TMA OFFRETITE DECOMPOSITION AND DTA CORRELATIONS

Weight loss (mg)[a]			Temperature range, °C	DTA correlations	Assignment
Sample 1	Sample 2	Sample 3[b]			
7.1	5.5	6.5	25–350	endo, 160°C	Loss of physically adsorbed H_2O
3.7	3.1	1.9	350–575	endo, 410°C	Decomposition of $(CH_3)_4N^+$
1.1	0.7	—	575–700	endo, 560°C	Dehydroxylation

[a] Initial weights of samples 1, 2, 3 were 69.5, 51.6 and 46.8 mg, respectively.
[b] Sample not heated above 600°C.

1.8, and 1.4 mg [calculated as $(CH_3)_3N$] for samples 1, 2, and 3, respectively. Using the stoichiometry from Eq. (1), together with the weight of $(CH_3)_3N$ evolved above, we find that the total amounts of expected products from samples 1, 2, and 3 are 3.4, 2.2, and 1.7 mg, respectively. This shows reasonably good agreement with the experimentally observed values (Table 4) over the temperature range 350–575°C. Dehydroxylation of the protonic sites created during tetramethylammonium ion decomposition contributes to the weight loss between 575° and 700°C. The endotherm in the DTA profile at 560°C is identified with this TGA weight loss.

3. Thermal analysis of ammonium and hydrogen form of synthetic offretite. The ammonium form of offretite, prepared by room temperature ion exchange, has a unit cell composition shown in Table 1. Results of DTA and TGA analyses are presented in Fig. 7. The NH_3 emerging from the effluent stream was also titrated with sulfamic acid. The milliliters of acid consumed and the corresponding weight loss during programmed heating are shown in Fig. 7A. In the temperature region 325 and 625°C of the thermogram we find excellent agreement between the observed weight loss, 1.6 mg of NH_3, and that calculated from the acid titration of NH_3 in the effluent stream, 1.5 mg. The loss of constitutive water (0.8 mg), between 600 and 700°C, agrees well with the value predicted from the amount of NH_4^+ which decomposed. The relatively slow loss of NH_3 followed closely by dehydroxylation of the zeolite resembles the behavior of NH_4T (*19*) and differs from that of NH_4Y (*20, 21*). The maximum rate of deamination, under identical calcination conditions, occurs at 325°C in the case of NH_4Y (*19*) and 425°C for NH_4T (*19*) and NH_4 offretite. Offretite seems to be functioning as a much stronger acid than NH_4Y.

We observed from the thermogram that a pure H form of offretite could be produced by programmed decomposition of NH_4 form up to 425°C the temperature of maximum NH_3 loss. Continued heating at this temperature, about 16 hr, should result in a catalyst essentially free of NH_4^+ but retaining all of its chemical water. This was verified by an *in situ* TGA calcination.

Figures 7B and 7C show DTA profiles recorded in N_2 and O_2 atmospheres. The exotherms (Fig. 7A) near 400° and 500°C, involving intracrystalline oxidation, are very similar to the profiles observed in NH_4-faujasite (*22*) and bentonite (*23*). Intracrystalline oxidation has also been observed in mordenite (*24*) and chabazite

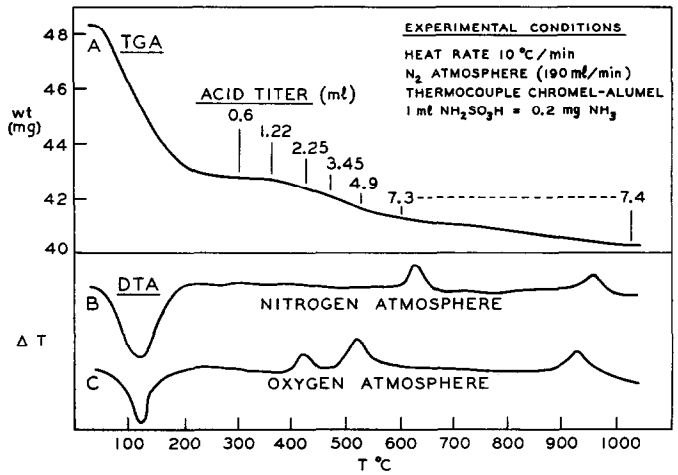

FIG. 7. Thermal analysis of NH_4-offretite: (A) thermogram of acid (NH_2SO_3H) titration, (B) DTA profile in N_2, and (C) in O_2 atmosphere.

(*24*). The weak exotherm at 963°C represents lattice collapse in NH_4-offretite at a temperature 100° lower than in the parent form.

Examination of the unit cell in NH_4-offretite, Table 1, indicates that there is a significant amount of potassium which remains after room temperature ion exchange. The K/Al ratio of 0.23 corresponds to about one potassium per unit cell. The resistance of this potassium ion to room temperature ion exchange is undoubtedly due to its strong bonding to the framework and/or its presence in a site which isolates it from the incoming exchangeable species. The hexagonal prisms (double six-membered ring) or the cancrinite cages, largest aperture about 1.8 Å in diameter, are the most probable locations for the residual potassium ion in offretite.

Catalytic Testing

Previous investigations (*25–28*) have described the catalytic hydrocarbon cracking activity of faujasite, zeolite A, ZK-5, natural mordenite and erionite. We have evaluated the catalytic activity of synthetic H-offretite for *n*-hexane cracking using the α test developed by Miale, Chen and Weisz (*29*). α is defined as the rate constant (rate of *n*-hexane conversion per unit volume) relative to that of a conventional silica-alumina cracking catalyst under standard conditions (*28*). The cracking activity of synthetic H-offretite (α = 4,200) is comparable to synthetic erionite (α = 4,175) (*18*) and NH_4-faujasite (α = 6,400) (*29*) and greater than that of ZK-5 (α = 450) (*30*) and H-mordenite (α = 2,500) (*30*).

Note added in proof: After this manuscript was submitted, two papers by Prof. R. M. Barrer and coworkers appeared in press [*J. Chem. Soc.* (A), 1470 (1970); *Trans. Farad. Soc.*, **66**, 1610 (1970)]. In review of their observations and after subsequent discussion with these authors, we find many correlations with our catalytic system.

ACKNOWLEDGMENTS

The authors are grateful to Mrs. M. K. Rubin for technical advice in the preparation of the zeolite, and to Mr. H. G. Doherty for performing the catalytic tests. Valuable suggestions and comments by Professor L. S. Bartell of the University of Michigan and Dr. D. H. Olson of Mobil Research and Development Corporation are gratefully acknowledged.

REFERENCES

1. GONNARD, F., *C. R. Acad. Sci.* **111,** 1002 (1890).
2. EAKLE, A. S., *Z. Kristallogr. Mineral.* **30,** 176 (1898).
3. STAPLES, L. W., AND GARD, J. A., *Mineral. Mag.* **32,** 261 (1959).
4. HEY, M. H., AND FEYER, E. E., *Mineral. Mag.* **33,** 66 (1962).
5. BENNETT, J. M., AND GARD, J. A., *Nature* **24,** 1005 (1967).
6. STRUNZ, H., *Naturwissenschaften* **47,** 59 (1960).
7. BARRER, R. M., AND PETERSON, D. L., *J. Phys. Chem.* **68,** 3427 (1964).
8. AMES, L. L., *Amer. Mineral.* **46,** 1120 (1961).
9. EBERLY, P. E., *Amer. Mineral.* **49,** 30 (1964).
10. DEFFEYES, K. S., *Amer. Mineral.* **44,** 501 (1959).
11. PIGUZOVA, L. I., BEZZUBOVA, I. M., VITUKHINA, A. S., DMITRIEVA, V. F., AND KRASNYI, E. B., *Vestsi. Akad. Navuk Belarus. SSR, Ser. Khim. Navuk* **59,** (1966).
12. ERMOLENKO, N. F., SHIRINSKAYA, L. P., AND ULASIK, T. G., *Dokl. Akad. Nauk Beloruss. SSR* **9,** 807 (1965).
13. ZHDANOV, S. P., AND NOVIKOV, B. G., *Vestsi Akad. Navuk Belaruss. SSR, Ser. Khim. Navuk* **44,** (1966).
14. NIKOLINA, V. YA., KNYSH, L. I., AND SOKOLOVA, N. A., *Vestsi Akad. Navuk Belaruss. SSR, Ser. Khim. Navuk* **65,** (1966).
15. ZHDANOV, S. P., AND NOVIKOV, B. G., *Dokl. Akad. Nauk. SSSR* **166,** 1107 (1966).
16. CHEN, N. Y., LUCKI, S. J., AND MOWER, E. B., *J. Catal.* **13,** 329 (1969).
17. RUBIN, M. K., German Patent P1806154.6, October 16, 1968.
18. WHYTE, JR., T. E., unpublished work.
19. KERR, G. T., unpublished work.
20. UYTTERHOEVEN, J. B., CHRISTNER, L. G., AND HALL, W. K., *J. Phys. Chem.* **69,** 2117 (1965).
21. CATTANACH, J., WU, E. L., AND VENUTO, P. B., *J. Catal.* **11,** 342 (1968).
22. VENUTO, P. B., WU, E. L., AND CATTANACH, J., *Anal. Chem.* **38,** 1266 (1966).
23. ELLIS, B. G., Ph.D. Thesis, Michigan State University, East Lansing, Mich., **1961.**
24. BARRER, R. M., *Nature* **164, 112 (1949).**
25. WEISZ, P. B., AND FRILETTE, V. J., *J. Phys. Chem.* **64,** 382 (1960).

26. FRILETTE, V. J., WEISZ, P. B., AND GOLDEN, R. L., *J. Catal.* **1,** 301 (1962).
27. WEISZ, P. B., FRILETTE, V. J., MAATMAN, R. W., AND MOWER, E. B., *J. Catal.* **1,** 307 (1962).
28. PLANK, C. J., ROSINSKI, E. J., AND HAWTHORNE, W. P., *Ind. Eng. Chem. Prod. Res. Develop.* **3,** 165 (1964).
29. MIALE, J. N., CHEN, N. Y., AND WEISZ, P. B., *J. Catal.* **6,** 278 (1966).
30. WEISZ, P. B., AND MIALE, J. N., *J. Catal.* **4,** 527 (1964).